Integration of ITER diagnostic ports at the Budker institute

A. Shoshin [a,e,*], A. Burdakov [a,f], M. Ivantsivskiy [a], R. Reichle [b], V. Udintsev [b], J. Guirao [b], S. Pak [b],
A. Zvonkov [c], D. Kravtsov [c], N. Sorokina [c], Y. Sulyaev [a,e], A. Listopad [a], D. Gavrilenko [a],
A. Taskaev [a], E. Shabunin [a], V. Seryomin [a], S. Shiyankov [a], E. Zaytcev [a], P. Seleznev [a],
A. Semenov [a,f], S. Polosatkin [a,e,f], S. Taskaev [a,e], D. Kasatov [a,e], I. Shchudlo [a,e], M. Bikchurina [e],
V. Modestov [d], A. Smirnov [d], A. Pozhilov [d], A. Lobachev [d], I. Loginov [d], O. Shagniev [d],
I. Kirienko [d], I. Buslakov [d]

[a] Budker Institute of Nuclear Physic SB RAS, Novosibirsk, Russia
[b] ITER Organization, Route de Vinon-sur-Verdon, France
[c] Institution Project Center ITER (RF DA), Moscow, Russia
[d] Peter the Great St. Petersburg Polytechnic University, St. Petersburg, Russia
[e] Novosibirsk State University, Novosibirsk, Russia
[f] Novosibirsk State Technical University, Novosibirsk, Russia

ABSTRACT

The paper presents results of the design development of the diagnostic equatorial and upper ports by RF DA (Russian Federation Domestic Agency) and results of the preparation of the production and assembly areas. The ports are being developed at the Budker Institute of Nuclear Physics of the Siberian Branch of the Russian Academy of Sciences (BINP) in good coordination with the ITER Central Team with the task of standardizing ports. Studies of boron carbide ceramics were conducted to prove that they meet the requirements of ITER. The preparation of port-plug production and the construction of the assembly hall at the BINP are described.

1. Introduction

The aim of the international project ITER is to demonstrate the feasibility of creating burning fusion plasmas with the release of large amounts of energy (up to 500–700 MW [1]). The plasma will be heated to very high temperatures inside the vacuum chamber. A very important task for understanding plasma processes and ensuring a safe discharge mode is to determine plasma parameters. For this purpose, a large number of diagnostics are being developed, which will be placed in the diagnostic ports of the vacuum chamber and will explore the plasma from different sides, are being developed. The diagnostic ports will also house various auxiliary equipment, such as plasma control systems suppressing plasma disruption. Three types of diagnostic ports are used to place diagnostic systems in the vacuum vessel: upper, equatorial and lower.

The design of the Diagnostic generic upper port plug (GUPP) and Diagnostic generic equatorial port plug (GEPP) is meant to be common to most upper and equatorial port-based diagnostic systems (see Figs. 1

and 2). It provides a common platform, or support/container, for a variety of diagnostics. In addition, the port plug structure must contribute to the nuclear shielding of the port and further contain circulated water to allow cooling during operation and heating during bake-out. The BINP develops a modular design in close cooperation with the ITER Central Team, specifically also the diagnostic port integration project team (DPI-PT), in the framework of port standardization [2–4]. The modular design allows the standardization of diagnostic ports developed in different countries, allowing the use of the same tools for the maintenance and repair of the ports, as well as the use of similar technologies for the production of port elements.

2. Description of the design and features of the diagnostic port plugs

The BINP is developing the ITER upper and equatorial ports in a unified approach: a modular design [2–4]. The in-vessel part of the diagnostic ports consists of the following main components: the

---
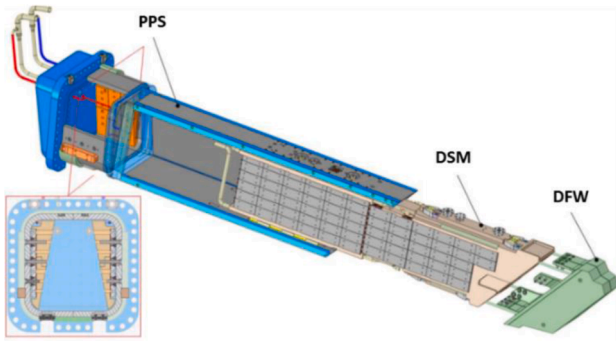
Fig. 1. Overview of the Generic Upper Port Plug structure with a modular configuration.
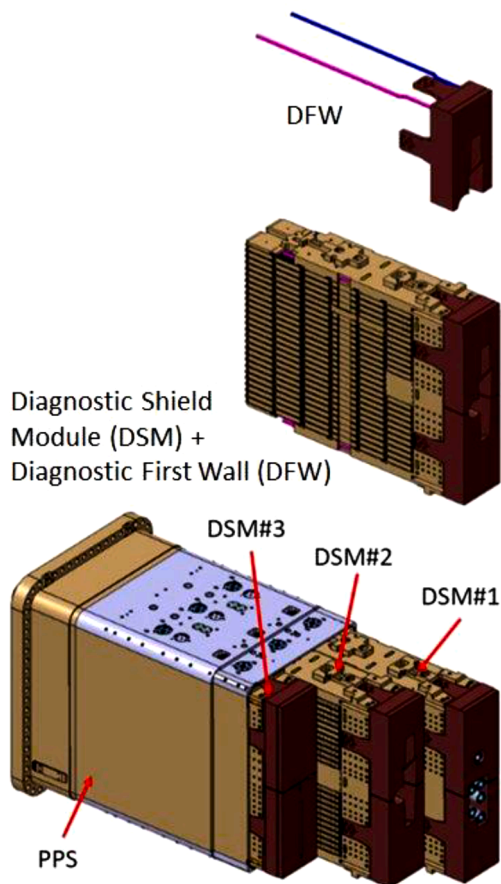
Fig. 2. Overview of Equatorial Port Plug #11 with a modular configuration.

diagnostic first wall (DFW), the diagnostic shielding module (DSM) and the port plug structure (PPS) (see Fig. 1). The DFWs and the PPSs are developed, customized as requested by the port integrator and supplied by other suppliers. The DFWs and the PPS will be joined together with the DSMs in the BINP's assembly hall. The DSM manufacture is the responsibility of the port integrator, the other two component types shall be developed and supplied by other suppliers.

Unlike the diagnostic upper port plugs, the diagnostic equatorial port plugs consist of three DSMs, which are oriented vertically (see Fig. 2).

The diagnostic ports should provide a 10^9-fold decrease in neutron flux—from 10^{14} n/cm^2·s on the Diagnostic First Wall to 10^5 n/cm^2·s in the Port Cell—and ensure that the dose rate near the closure plate will be below 100 μSv/h 12 days after reactor shutdown [2,3]. Radiation protection is a dramatically complicated issue as the ports have stringent

weight restrictions: an equatorial port may not be heavier than 45 tons and a single DSM may not be heavier than 10 tons. The BINP, the ITER Central Team, and the US Domestic Agency independently proposed boron carbide for port protection because of its low density and high neutron capture cross-section. The ITER Central Team also performed comparative radiation shielding calculations for a large number of materials (metals, concretes, polymers, boron compounds, water, to name some), ensuring that the fillers had the same weight [5]. The report concluded that boron carbide is one of the best options for ITER [5].

Initially, the BINP suggested pouring boron carbide powder into closed boxes which have cutouts for diagnostics (Fig. 3, left). However, this approach was finally not selected by the ITER Vacuum Section, and so it was proposed to use boron carbide ceramics. The BINP suggested using ceramic blocks of the simplest possible design: rectangular blocks without cutouts, as they are the cheapest to produce, but require a metal framework. A prototype of such a neutron shielding arrangement was made. However, after discussions with the ITER Central Team, it was decided to change to using flat shielding trays with centrally holed ceramic blocks attached to them on both sides (Fig. 3, right).

Each DSM is integrated using tenant diagnostics constraints defined in the Interface Sheets and CAD models following the generic Modular DSM design gaps and tolerances between items inside the Port Plug. The latter are managed by shielding trays to avoid additional nuclear fluxes following the ALARA (As Low As Reasonably Achievable) principle. The closure plate of the Port Plug is one of the key design drivers of EP #11 integration. There are apertures and cut-outs both on the Port Plug closure plate and in the inner part of the Bioshield Plug. Each diagnostic system provides information on what interfaces they need on the closure plate, such as windows, feedthroughs, or direct access to the vacuum vessel. One electrical feedthrough is shared between tenants and port plug structures.

The DSM consists of a C-shaped metal frame with vertical blades inside (size 2.3·2.0·0.52 m), see Fig. 4. This design provides the necessary rigidity and structural integrity irrespective of the internal location of the diagnostics [6].

On the vertical blades around the diagnostics, there are metal trays with B$_4$C ceramic blocks. To eliminate gaps between the trays and diagnostics equipment, stainless steel blocks are used as backfilling units. They are installed on the DSM and fill its empty space (see Fig. 4).

The major issue was the need to prove the feasibility of using a large number of boron carbide ceramic bricks in the ITER vacuum.

The redesign of the DSM upper ports led to a change in their classification according to the French Order on Pressurized Nuclear Equipment (ESPN Order). The assessment [8] shows that the DSM of Upper Ports #02 and 08 should be reclassified as ESP Pressure Category III (without changes) and Level N3 (formerly Level N2 in the Procurement Arrangements).

All design activities were supported by mechanical, hydraulic and

Fig. 3. Drawing of the previous design steel box with boron carbide powder for DSM Equatorial Port Plug #11 with cutouts for diagnostics (left) and a photo of the prototype tray in its current design (right). For better thermal conductivity, the tray in the prototype was made of bronze; however, calculations showed that bronze would not withstand expected loads, and for that reason it was decided to use steel 316L(N)-IG instead.
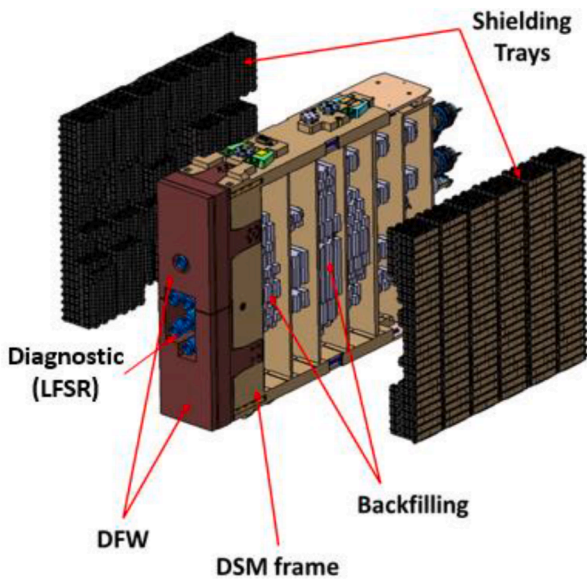
Fig. 4. Exploded-view drawing of the shielding design of Equatorial Port Plug #11 DSM #1. LFSR: Low-Field Side Reflectometer [7].

thermal analyses performed by the St. Petersburg Polytechnic University (SPbPU) [3–4,8–10]. Fig. 5 shows the calculation of the electromagnetic loads on the upper port at one type of disruption, a Vertical Disruption Event type III [11]. The results were expertized by the ITER Organization during design reviews, with the diagnostic teams contributing and the applicability of the diagnostic ports confirmed.

3. Tests of boron carbide ceramics (shielding bricks)

Boron carbide (B_4C) ceramic bricks are located inside the port plugs for neutron shielding. Since a huge number of bricks are located in the vacuum, the main requirement on the ceramics is its low outgassing rate, which is regulated by the ITER Vacuum Handbook (IVH) [12] and the approved specification for the supply of B_4C [13]. According to the recommendation of the ITER Organization set out in the specification, the outgassing rate of ceramics is limited to $1 \cdot 10^{-8}$ Pa·m^3·s^{-1}·m^{-2} for hydrogen [13].

Russian manufacturers of ceramics, with Virial Ltd. (St. Petersburg) one of them, submitted samples and the BINP has conducted numerous studies on the chemical composition, thermal and vacuum properties of the ceramics, the results of which are presented in the Ref. [14–16]. In particular, a long-term vacuum test was carried out, when large amounts of the sintered ceramics were not removed from the vacuum stand for 2.5 years and measurements were regularly carried out. The table with
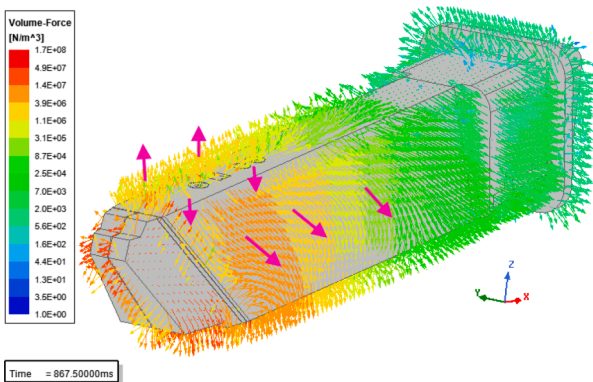
the results of measurements over the first year is presented in Ref. [15]. The results of recent measurements are as follows: after 20 months, the outgassing rate was $2.78 \cdot 10^{-9}$ Pa·m^3·s^{-1}·m^{-2}; after 25 months, it was $2.21 \cdot 10^{-9}$ Pa·m^3·s^{-1}·m^{-2}; and after 30 month, it decreased 5-fold, to $2.06 \cdot 10^{-9}$ Pa·m^3·s^{-1}·m^{-2} from the initial value. The measured spectrum of gasses is shown in Fig. 6. The spectrum meets the requirements of the IVH general test for cleanliness.

An important requirement on boron carbide ceramics (B_4C) is the minimum amount of hazardous impurities. The presence of impurities worsens the vacuum properties of the material and leads to increased radioactivity after neutron irradiation. A direct and sensitive method for measuring impurities leading to activation is to measure the gamma spectra of the activated substance after irradiation with neutrons with a spectrum similar to the neutron spectrum at the location of the ceramic bricks in the port plug. Such a high-intensity neutron spectrum can be obtained on a powerful tandem accelerator in the BINP (Novosibirsk) [17]. The results of experiments with irradiation of ceramics with low-energy neutrons are presented in Ref. [14]; the results of experiments with fast neutrons are presented in Ref. [15] and are shown in Fig. 7.

The ITER organization calculated the rate of formation of helium and tritium in EPP#11 (Equatorial Port Plug) elements, which showed that in the first column of ceramics the amount of helium was 10^{18} atoms/cm^3, and in the last column, 10^{14} atoms/cm^3. The amount of tritium was 10^{16} atoms/cm^3 in the first column of ceramics and 10^{11} atoms/cm^3 in the last column [18]. Thus, boron burnout after the SA-2 scenario of ITER operation [1] is negligible.

Studies have shown that boron carbide ceramics meet all ITER requirements for vacuum properties and radiation safety.

In addition to neutron shielding, boron carbide has also been proposed for fusion reactors as a first wall coating [19]. The BINP has extensive experience in researching the durability of the first wall to powerful heat fluxes [20–27]. Now the BINP is conducting experiments to study the rapid heating of boron carbide ceramic samples by a powerful laser pulse, and the results will be published later. Similar research is conducted with plasma guns [28].

4. Manufacturability

As a part of the preparation for the production of diagnostic port components, a series of technological studies was carried out both by the BINP and by the ITER Organization to confirm the feasibility of using the proposed technologies for the manufacture of the components. A typical cooling system has been developed for the DSM of the equatorial and upper ports. A prototyping of complicated assemblies was carried out, including the manufacture of gun-drilled channels and the welding of

Fig. 5. Maximum electromagnetic force density profile in the Upper Port #07 components during a type III Vertical Disruption Event, N/m^3 [11].
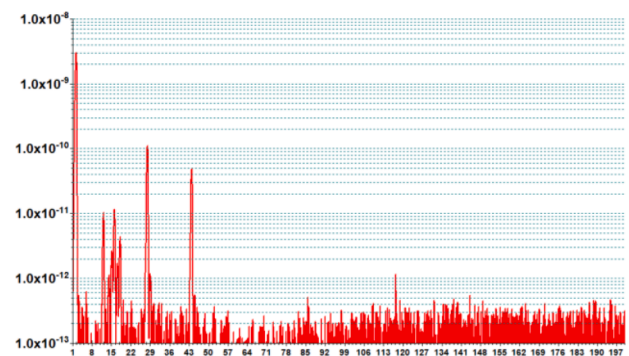
Fig. 6. Mass spectrum of gasses measured with a quadrupole mass spectrometer for Virial-sintered boron carbide ceramics at 100 °C after 2.5 years in the vacuum. On the vertical axis: the partial pressure in torr; on the horizontal axis: the atomic mass. Masses (a.u.m.) and components of the six highest peaks: 2 H_2, 12 C, 16 O, 18 H_2O, 28 CO, 44 CO_2.
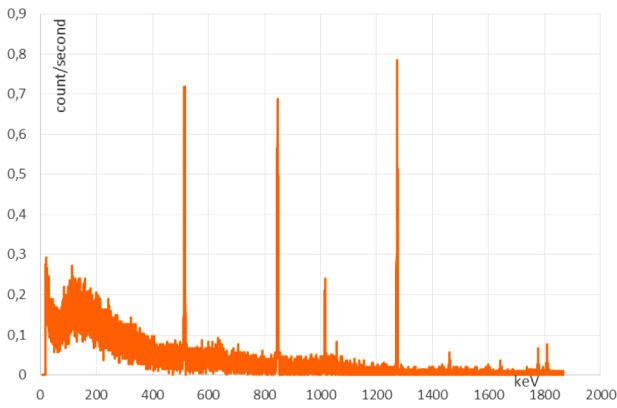
Fig. 7. Measured spectrum of gamma rays emitted by sintered boron carbide ceramics (Virial) after fast neutron irradiation. On the vertical axis: the number of detector counts; on the horizontal axis: photon energy in keV.

blind holes.

The DSM structure needs an active cooling system to allow cooling during operation and heating during bake-out. The total mass flow rate available for EPP #11 is 22.2 kg/s [10]. The parameters of the water cooling channels were carefully calculated taking into account the ITER requirements and heat release during the DT discharge [10]. For active cooling, the DSMs have a branching network of cooling channels (see example in Fig. 8), some of them are up to 2 m long. To produce this kind of channels, gun-drilled holes 10, 15, 20, 25 mm in diameter are required.

The DSM cooling system contains multiple orifices, which are used to balance mass flows inside the DSM and between the DSM and the DFW. The SPbPU conducted an analysis; proper values of the hydraulic resistance coefficient of the orifices and the corresponding dimensions of the orifices were determined [29].

As was demonstrated on the prototypes, it is possible to deep-drill cooling channels; additionally, a technology for measuring the straightness of these channels and a technology for welding plugs of these channels were developed.

The next critical issues after drilling that kind of channels are the welding and inspection of channel caps. According to the requirements

from IVH [12] and RCC-MR 2007 code, all hermetic welds should have full-penetration welds and 100% non-destructive testing (NDT) inspection (X-ray or ultrasonic testing). Because the network of cooling channels has several layers and the thickness of DSM parts in some areas is 350–500 mm, X-ray cannot be applied to these types of welds. Instead, a special design of cups has been prepared (see Fig. 9).

To demonstrate the feasibility of an ultrasonic inspection, some R&D has been carried out. A local full-scale mock-up has been designed and manufactured.

Another important issue with relevance to successful port integration is the welding of diagnostic flanges to the port plug structure at the closure plate. The main challenge here is how to complete full-penetration welding and inspection in the settings of great constraints. The closure plate is a vacuum border of a port plug structure. All flanges from tenant diagnostics and all necessary services should penetrate a vacuum border through the closure plate. That is why the closure plate is a quite complicated safety important component with great restrictions. For successful welding on the closure plate, the BINP plans to use

Fig. 8. Geometry of the cooling channels of Equatorial Port Plug #11 DSM #2 and flow direction (drilled channels + pipes) [10]. The front of the DSM has more energy release, hence a large number of water channels running through the DSM frame (Fig. 3). The flow rate was 0.09 kg/s in each of the ten channel in vertical plates.
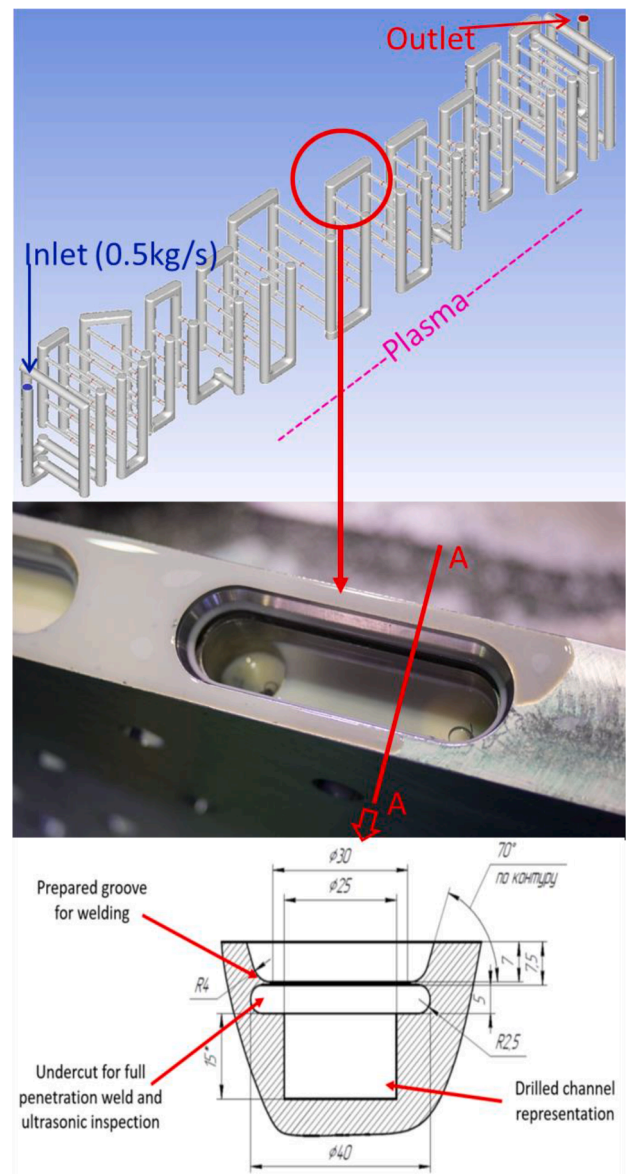
Fig. 9. Shape of the water channels in the front of the DSM (top), part of the full-size mock-up of the water channels for development of welding plugs during manufacturing (center) and a drawing of a cooling channel cap cross-section (bottom).

automatic tungsten inert gas (TIG) orbital welding (see Fig. 10). This type of orbital welding provides welding from the internal part of the flanges and helps to deal with the inaccessibility of some sites. The feasibility of this kind of welding has preliminarily been demonstrated on a flange mock-up (see Fig. 10).

While preparing for port-plug production, the BINP developed and agreed with the ITER Organization documents by approval of related documents for manufacturing, gun-drilling, handling [30], storage, cleaning [31] and labeling of ITER parts.

5. Assembly hall

An important task in preparing for the production of the ITER port-plugs is the creation of a special assembly hall at the BINP (see Fig. 11). This hall should provide the ability to assemble heavy and large-sized port elements, for flange welding on the closure plate, for installation and alignment of diagnostics.

The main technological requirements are that the premises should be level I work areas according to the RCC-MR code at all times during all assembly operations and testing (see Fig. 11) and that acceptance tests should be carried out in a clean room environment.

Critical restrictions for the creation of the assembly hall are the weight of the equatorial port plug, which is 48 tons and the length of the upper port plug, which is about 6 m. To assemble the upper port plug, the necessary space under the crane hook should be at least 13 m (see Fig. 11). Since the assembly and installation of different equipment (DFW, PPS, diagnostic components) will be occurring at different times, sometimes together with the assembly of port-plugs, the hall must be re-
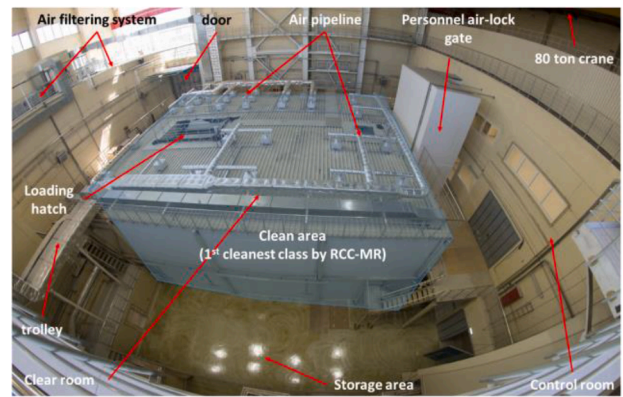
Fig. 11. Assembly hall overview.

arranged to allow different components to be transported and stored independently of each other (see Fig. 12). A clean room in the assembly hall has been designed, constructed and passed through the clean acceptance test (see Fig. 13). The clean area consists of three isolated clean rooms (Fig. 12), whose dimensions allow for simultaneous assembly of 2 DSMs and 2 port-plugs. The central clean room is for loading the equipment, washing it and welding the flanges. One isolated room has a higher cleanliness class (class 6 according to ISO 14,644–1) for assembly of optical diagnostics.

The graph in Fig. 13 presents the time dependence of the number of dust particles (5 micrometers) per m^3 inside the clean area of the assembly hall. At 13:00, the Acceptance Commission participants enter the first clean work area; at 13:20, the second. During inspection, up to 10 persons were in the clean room. The number of particles was increased, but was still lower than their maximum allowable number for this cleanliness class (3000 particles per m^3). Special equipment has been developed for canting and tilting and working with large-sized and heavy port parts (see Fig. 14).
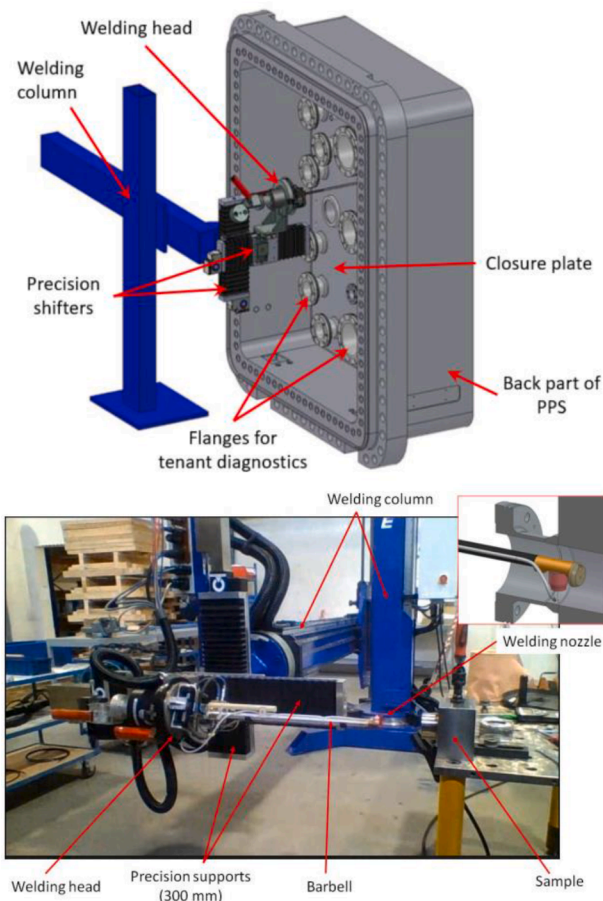
Fig. 10. Elements interfering with the welding process on the closure plate (above); demonstration of the feasibility of internal welding on the flange mock-up (below).
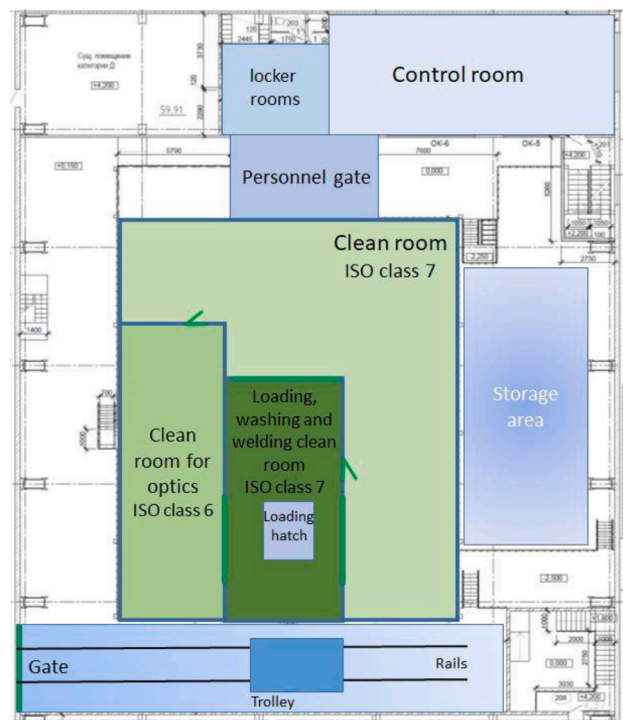
Fig. 12. Layout of the assembly hall and clean rooms.
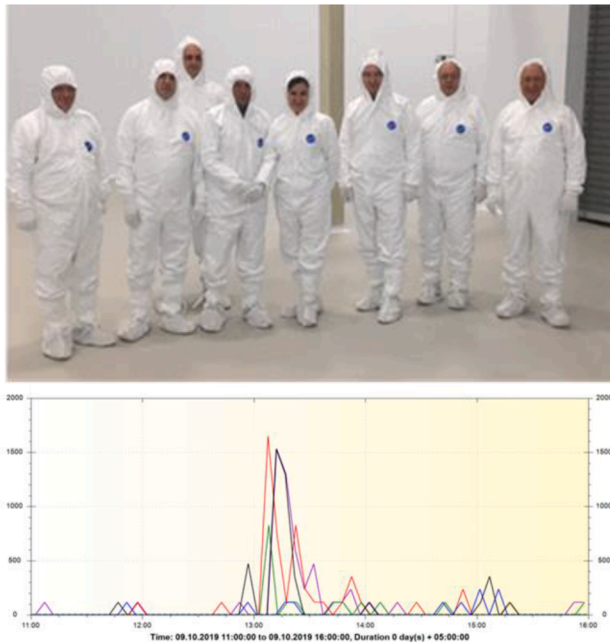
Fig. 13. Acceptance test of the clean room in the assembly hall: Acceptance Commission participants (above); time dependence of the number of dust particles (5 micrometers) per m^3 (bottom).

Fig. 14. Clean room in the BINP with port plug handler inside (top) and DSM equatorial port handler installed (bottom).

6. Conclusion

Integration of the diagnostic equatorial and upper ports developed by RF DA has demonstrated the applicability of a single unified principle: a modular design of diagnostics ports.

The possibility of using large amounts of boron carbide ceramics in ITER diagnostic ports has been demonstrated.

Manufacturing techniques for supporting the design solutions have been developed and demonstrated.

A specialized assembly hall was built that successfully passed the cleanliness test; now it is fully operational.

CRediT authorship contribution statement

A. Shoshin: Investigation, Writing – original draft, Writing – review & editing. **A. Burdakov:** Conceptualization, Writing – original draft, Writing – review & editing, Supervision. **M. Ivantsivskiy:** Conceptualization, Writing – original draft, Writing – review & editing, Supervision. **R. Reichle:** Validation. **V. Udintsev:** Validation. **J. Guirao:** Validation. **S. Pak:** Validation. **A. Zvonkov:** Validation. **D. Kravtsov:** Validation. **N. Sorokina:** Validation. **Y. Sulyaev:** Investigation. **A. Listopad:** Investigation. **D. Gavrilenko:** Investigation. **A. Taskaev:** Investigation. **E. Shabunin:** Investigation. **V. Seryomin:** Investigation. **S. Shiyankov:** Methodology. **E. Zaytcev:** Methodology. **P. Seleznev:** Methodology. **A. Semenov:** Investigation, Formal analysis. **S. Polosatkin:** Investigation, Formal analysis. **S. Taskaev:** Investigation, Formal analysis. **D. Kasatov:** Investigation, Formal analysis. **I. Shchudlo:** Investigation, Formal analysis. **M. Bikchurina:** Investigation, Formal analysis. **V. Modestov:** Software, Formal analysis. **A. Smirnov:** Software, Formal analysis. **A. Pozhilov:** Software, Formal analysis. **A. Lobachev:** Software, Formal analysis. **I. Loginov:** Software, Formal analysis. **O. Shagniev:** Software, Formal analysis. **I. Kirienko:** Software, Formal analysis. **I. Buslakov:** Software, Formal analysis.

Declaration of Competing Interest

The authors declare that they have no known competing financial interests or personal relationships that could have appeared to influence the work reported in this paper.

Acknowledgments

References

[1] Recommendation on Plasma scenarios, (2009) ITER_D_2V3V8G.
[2] J. Guirao, M.J. Walsh, V.S. Udintsev, et al., Standardized integration of ITER diagnostics Equatorial Port Plugs, Fusion Eng. Des. 146B (2019) 1548–1552, https://doi.org/10.1016/j.fusengdes.2019.02.126.
[3] Yu.S. Sulyaev, E.V. Alexandrov, A.V. Burdakov, et al., Engineering Calculations and Preparation for Manufacturing of ITER Equatorial port #11, IEEE T. Plasma Sci. 48 (6) (2020) 1631–1636, https://doi.org/10.1109/TPS.2020.2985113.
[4] A. Listopad, E. Alexandrov, A. Burdakov, et al., Preliminary design of the ITER upper ports #02 and #08 integration, IEEE T. Plasma Sci. 48 (6) (2020) 1721–1725, https://doi.org/10.1109/TPS.2020.2985401.
[5] Comparison of materials for neutron shielding for the Diagnostic Shielding Modules, (2014) ITER_D_LA8JV5.
[6] 55.QB - Structural integrity report for In-PP components, (2021) ITER_D_35JX3U.

[7] W. Wang, A. Zolfaghari, H. Neilson, et al., Thermal loads and cooling design for ITER in-Port Low field side reflectometer diagnostic system, Fusion Eng. Des. 146B (2019) 1295–1299, https://doi.org/10.1016/j.fusengdes.2019.02.062.

[8] 55.U8 - Summary Report(s) justifying ESP(N) systems and components classification, (2021) ITER_D_VQ9X69.

[9] 55.QB - Electromagnetic analysis of EPP#11 for in-PP components, (2020) ITER_D_SSMM2V.

[10] 55.QB - Thermal loads and thermal, hydraulic and pressure analyses DSM-2, (2021) ITER_D_W62T2U.

[11] 55.U4/U5/U6/U7 - EM Loads calculations and analyses, (2021) ITER_D_23J2DU.

[12] ITER Vacuum Handbook, https://www.iter.org/technical-reports, Reference: ITR-19-004 (2019).

[13] 55.QB Material Specification for the supply of Boron Carbide (B4C), (2021) ITER_D_457TBH.

[14] A. Shoshin, A. Burdakov, M. Ivantsivskiy, et al., Qualification of boron carbide ceramics for use in ITER ports, IEEE T. Plasma Sci. 48 (6) (2020) 1474–1478, https://doi.org/10.1109/TPS.2019.2937605.

[15] A. Shoshin, A. Burdakov, M. Ivantsivskiy, et al., Test results of boron carbide ceramics for ITER port protection, Fusion Eng. Des. 168 (2021), 112426, https://doi.org/10.1016/j.fusengdes.2021.112426.

[16] A. Shoshin, A. Burdakov, M. Ivantsivskiy, et al., Properties of boron carbide ceramics made by various methods for use in ITER, Fusion Eng. Des. 146B (2019) 2007–2010, https://doi.org/10.1016/j.fusengdes.2019.03.088.

[17] S. Taskaev, E. Berendeev, M. Bikchurina, et al., Neutron source based on vacuum insulated tandem accelerator and lithium target, Biology (Basel) 10 (5) (2021) 350, https://doi.org/10.3390/biology10050350.

[18] Determination of quantities in EP#11 during machine operation, (2020) ITER_D_Y86WVS.

[19] L.B. Begrambekov, O.I. Buzhinskij, Features and advantages of boron carbide as a protective coating of the tokamak first wall, Plasma Devices Operat 15 (3) (2007) 193–199, https://doi.org/10.1080/10519990701450657.

[20] A.A. Shoshin, et al., Study of plasma-surface interaction at the GOL-3 facility, Fusion Eng. Des. 114 (2017) 157–179, https://doi.org/10.1016/j.fusengdes.2016.12.019.

[21] A.A. Shoshin, et al., Structure modification of different graphite and glassy carbon surfaces under high power action by hydrogen plasma, Fusion Sci. Technol. 59 (1T) (2011) 268–270, https://doi.org/10.13182/FST11-A11631.

[22] A. Huber, et al., Combined impact of transient heat loads and steady-state plasma exposure on tungsten, Fusion Eng. Des. 98-99 (2015) 1328–1332, https://doi.org/10.1016/j.fusengdes.2015.01.028.

[23] A.A. Shoshin, et al., Modification of preheated tungsten surface after irradiation at the GOL-3 facility, Fusion Eng. Des. 113 (2016) 66–70, https://doi.org/10.1016/j.fusengdes.2016.10.010.

[24] A.A. Vasilyev, et al., In-situ imaging of tungsten surface modification under ITER-like transient heat loads, Nucl. Mater. Energy 12 (2017) 553–558, https://doi.org/10.1016/j.nme.2016.11.017.

[25] L.N. Vyacheslavov, et al., Diagnostics of the dynamics of material damage by thermal shocks with the intensity possible in the ITER divertor, Phys. Scr. 93 (2018), 035602, https://doi.org/10.1088/1402-4896/aaa119.

[26] A.A. Vasilyev, et al., Continuous laser illumination for in situ investigation of tungsten erosion under transient thermal loads, Fusion Eng. Des. 146B (2019) 2366–2370, https://doi.org/10.1016/j.fusengdes.2019.03.192.

[27] L. Vyacheslavov, et al., In situ study of the processes of damage to the tungsten surface under transient heat loads possible in ITER, J. Nucl. Mater. 544 (2021), 152669, https://doi.org/10.1016/j.jnucmat.2020.152669.

[28] O.I. Buzhinskij, et al., B4C protective coating under irradiation by QSPA-T intensive plasma fluxes, Probl. Atom. Sci. Tech., Series Thermonuclear Fusion 38 (2) (2015) 32–38, https://doi.org/10.21517/0202-3822-2015-38-2-32-37.

[29] 55.QB – Analyses for determination of hydraulic resistance coefficient of orifices DSM-2, (2021) ITER_D_6EE99E.

[30] 55.QB - Cleaning procedure, (2021) ITER_D_4ZDXTA.

[31] 55.QB - Handling procedures, (2021) ITER_D_4ZDTVA.